JOURNAL OF PROPULSION AND POWER
Vol. 17, No. 2, March–April 2001

Plasma Confinement in the Whistler Wave Plasma Thruster

B. W. Stallard* and E. B. Hooper Jr.†
Lawrence Livermore National Laboratory, Livermore, California 94551
and
J. L. Power‡
NASA John H. Glenn Research Center at Lewis Field, Cleveland, Ohio 44135

Plasma thruster experiments using whistler wave plasma heating of electrons have shown large increases in the operating density and the plasma potential providing for ion acceleration when the edge potential was controlled through use of electrically floating electrodes at the plasma edge. Analysis of these results show that $E \times B$ (vector cross product) drifts within the radial electric field in the small diameter plasma column dominated the ion confinement and power balance. Measurements of a density increase at higher magnetic field are consistent with the predictions of ion orbit analysis. Device modifications to improve thruster performance are discussed.

Nomenclature

A_{eff}	=	effective gas box area for ion current flow
A_i	=	ion atomic weight
a	=	plasma radius
$B_{\text{mid}}\,(B_{\text{gb}})$	=	magnetic field at midfield (gas box)
B_{res}	=	magnetic field for electron cyclotron resonance, T
B_z	=	axial magnetic field component
E_i	=	exhaust plume ion energy, eV
$\langle E_i \rangle$	=	exhaust plume average ion axial energy, eV
E_r	=	radial electric field
e	=	electron charge, 1.602×10^{-19} C
$F(E_i)$	=	plume ion energy spectrum, eV/V
f	=	rf generator frequency, Hz
f_{relax}	=	bimodal relaxation frequency, Hz
I_{itot}	=	total gas box propellant ion current, A
I_p	=	probe current, A
J_{ep}	=	probe electron current density
$J_{\text{i-gb}}$, $J_{\text{i-mid}}$, $J_{\text{i-pl}}$	=	probe ion current density at gasbox, midplane, and plume
$J_{\text{i-sat}}$	=	probe ion saturation current density
m_e	=	electron mass, 9.1066×10^{-31} kg
m_i	=	ion mass
N	=	number of ion $E \times B$ (vector cross product) drift orbit radii in radius a
$n_e\,(n_i)$	=	electron (ion) density
n_{ec}	=	electron critical density
P_{iex}	=	exhaust plume ion power, W
R_p	=	Langmuir probe radius
r_0, r_{tp}	=	ion birth radius, maximum turning point radius
T_e	=	electron temperature, eV
V_r	=	plume probe repeller voltage, V
$\langle W_{i\perp} \rangle$	=	orbit-averaged, ion perpendicular drift energy, eV
Z	=	propellant ion charge state
ΔW_{ie}	=	mean ionization energy per electron–ion pair, eV
Δz_{pl}	=	plume probe distance, 0.35 m
$\Delta\Phi$	=	floating potential difference between on-axis and the boundary, V
ε_0	=	vacuum dielectric constant, 8.854×10^{-12} F/m
λ_{cx}	=	mean free path for ion charge exchange
λ_0	=	neutral mean free path for electron impact ionization
ρ_d	=	ion $E \times B$ drift orbit radius
ρ_i	=	ion Larmor radius
Φ_s	=	plasma sheath potential, V
Φ_0, Φ_b	=	plasma floating potential on-axis and at the boundary, V
$\phi_{\text{min}}\,(\phi_{\text{max}})$	=	minimum (maximum) floating potential in bimodal states, V
ω_{ci}	=	ion cyclotron frequency, Hz

Subscripts

$e(i)$	=	electron (ion)
gb (mid, pl)	=	gas box (midfield, plume) probe locations

I. Introduction

FOR long-range space missions, such as an interplanetary trip to Mars or to the outer solar system, reduced flight times, reduced propellant mass requirements, and improved energy efficiencies are possible with higher specific impulse I_{sp}. Electrical-propulsion methods, which accelerate propellant ions to large velocity, and plasma-based devices, which use hot plasmas to provide the energetic exhaust, offer the prospect of much higher I_{sp}. A variety of approaches have been tested in the laboratory, and a number of low-power devices have been used operationally in space (see Ref. 1 for an overview). Near-Earth orbit applications include satellite station keeping and orbit raising or correction.[1] Some thruster examples are resistojets, arcjets, magnetoplasmadynamic (MPD) thrusters, Hall effect accelerators, and ion engines (acceleration through electrically biased grids). NASA's deep space flight mission with the New Millennium Deep Space 1 spacecraft, launched in October 1998 with an ion engine for propulsion, is an example of electric propulsion for solar system exploration.[2] Because the power P to thrust T ratio scales $P/T \sim I_{\text{sp}}$, and because the power output of an onboard electrical power plant is likely to be much smaller than the thermal power of a large chemical rocket, a high I_{sp} thruster will produce much lower thrust. Consequently, it must operate for extended duration (up to thousands of hours). To satisfy this requirement, radial losses of plasma particles and energy within the thruster must be low to ensure low plasma erosion of material surfaces. Low radial losses, that is, good plasma confinement in the radial direction, also permit high-energy and propellant use efficiencies.

In this paper we discuss plasma-based propulsion using electron-cyclotron resonance heating (ECH) of plasma electrons by the whistler wave.[3,4] Previous thruster work with electron heating was carried out in the 1960s and more recently.[5–7] These thrusters also used electrodeless coupling of the rf power source to the whistler

Received 8 March 1999; revision received 19 April 2000; accepted for publication 1 June 2000.

*Physicist, Magnetic Fusion Energy, Laser Directorate, Box 808, L-637.
†Deputy Associate Director for Magnetic Fusion Energy (acting), Laser Directorate, Box 808, L-637. Senior Member AIAA.
‡Aerospace Engineer (retired), Board Propulsion Branch, Space Propulsion Technology, M/S 16-1. Member AIAA.

wave through a waveguide window and acceleration of heavy noble gases was studied. In many of these experiments, the thrust efficiency was low, and it appeared that diffusion of plasma across magnetic field lines to the wall of the devices limited performance.

For our thruster work, particle-in-cell code (PIC) modeling of the device has been described in Ref. 8, and the experimental status of our approach has been previously reported.[9] Here we update our interpretation of these results.[10] As previously described,[9] this method offers some potential advantages for extended duration and high-power-density operation. Among these are 1) smaller wall losses and wall sputtering through helix antenna coupling of the microwave heating power, 2) large power densities (kilowatt per square centimeter), obtained by generating the ion accelerating electric field within the plasma itself, and 3) variable I_{sp} through control of the plasma potential.

In brief, the principle of this approach is the following. Within a high-magnetic-field region, an antenna surrounding a plasma column couples a whistler wave into the plasma. The whistler wave at frequency f propagates along the column as it expands into weaker magnetic field, where it is absorbed at an electron-cyclotron resonance, defined by $B_{res} = 2\pi f/em_e$, thereby increasing the perpendicular energy of the electrons. The ∇B forces accelerate the heated electrons down the field, and, in turn, the ions are accelerated out the end of the thruster by the plasma potential that arises to maintain charge neutrality. Because the accelerating electric field is created in situ in the plasma, there are no grid–electrode plasma interactions. Producing thrust by accelerating ions with in situ potentials may be more energetically efficient than direct ion heating within the thruster, followed by expulsion out the nozzle. If cold ions are accelerated as they exit the nozzle, power losses to the walls can be small. If ions are heated before expulsion, large wall losses may arise from charge exchange of the heated ions on the injected propellant gas, unless preionization of the propellant gas is done.

By the use of the whistler wave, high plasma operating density is possible at low rf frequency. Whistler waves, launched into the plasma from a region at higher magnetic field than the electron resonance ($B > B_{res}$), are accessible to the resonant surface at plasma densities much greater than the critical density defined by $n_{ec} = (m_e\varepsilon_0/e^2)(4\pi^2 f^2)$. Such heating is overdense relative to the critical density in the sense that electromagnetic waves launched from $B < B_{res}$, are cutoff when $n_e > n_{ec}$.

During recent experiments we measured extracted ion energies in the exhaust plume up to 150 eV, consistent with the measured plasma floating potentials.[9] Because the ion species mix of the exhaust plume plasma was not measured, the I_{sp} is uncertain. For evaluation of formulas in this paper, we assumed molecular hydrogen ions H_2^+ ($Z = 1$ and $A_i = 2$). Thus, for H_2^+, 150-eV directed ion energy corresponds to $I_{sp} \approx 12{,}000$ s. Typical operating parameters were plasma density at the resonance up to $1\text{–}2 \times 10^{12}$ cm^{-3} and electron temperature in the range $T_e \sim 10\text{–}20$ eV. However, ion extraction efficiencies for the plasma exhaust plume were low (<5%), and we report here the conclusion that poor radial confinement was a probable explanation for the low efficiency. As concluded in this paper, the low efficiency most likely results from large ion drift orbits, driven by large radial electric field E_r, which lead to radial loss of power and particles. Similar large orbit losses were probably important in earlier ECH-driven thrusters because heavy ions in small radius plasmas were employed.[5] Also note that the radial electric field plays an important role in plasma confinement in toroidal plasmas and is an major area of study, although in these plasmas sufficiently large plasma flows related to E_r can improve confinement through turbulence suppression.[11]

In Sec. II, we describe thruster operation and compare improvements in the operating density and potentials of the device when we controlled the plasma edge potentials. In Sec. III, the role of the radial electric field E_r in controlling radial transport and power balance is discussed. Finally, in Sec. IV, we summarize our results and discuss several thruster modifications designed to improve efficiency.

II. Thruster Operation with Boundary Potential Control

A. Description of Experiment

A description of the experimental device and preliminary results were described in Ref. 9. Figure 1 here shows the geometry of the thruster. The principle components include 1) two magnet coils to provide a uniform region of high magnetic field and a magnetic nozzle to exhaust the plasma; 2) a double-feed, bifilar helix antenna, surrounding a 5-cm-diam quartz tube, which was used to launch the whistler wave; 3) a propellant feed chamber (designated gas box or gb), surrounding the expanding plasma column, for injecting propellant gas and which encloses the electron cyclotron resonance surface; and 4) locations of various plasma diagnostic probes. Propellant gas was injected only into the gas box. Also shown are several metal plasma boundary electrodes: two radial edge limiters, a propellant feed baffle consisting of nine connected chambers mounted inside the gas box and closely surrounding the plasma column, and an end wall disk electrode. The radial limiters were located at the end of the quartz tube (designated the midfield or mid limiter) and at the output of the gas box (downstream limiter). Propellant gas entered into the propellant feed baffle from the gas box through an annular slot in one chamber. The baffle was supported from the downstream limiter, but was electrically isolated from it. Its purpose was to increase the gas density within the electron-resonance region to increase gas ionization efficiency.

Electrical leads, individually connected to each limiter, to the propellant feed baffle and to the end electrode could be either grounded or allowed to float electrically during operation. The limiter electrodes and propellant feed baffle were used to control the radial electric fields within the plasma column. The experiment was run in a pulsed mode and was powered by a 30-kW, 915-MHz magnetron.

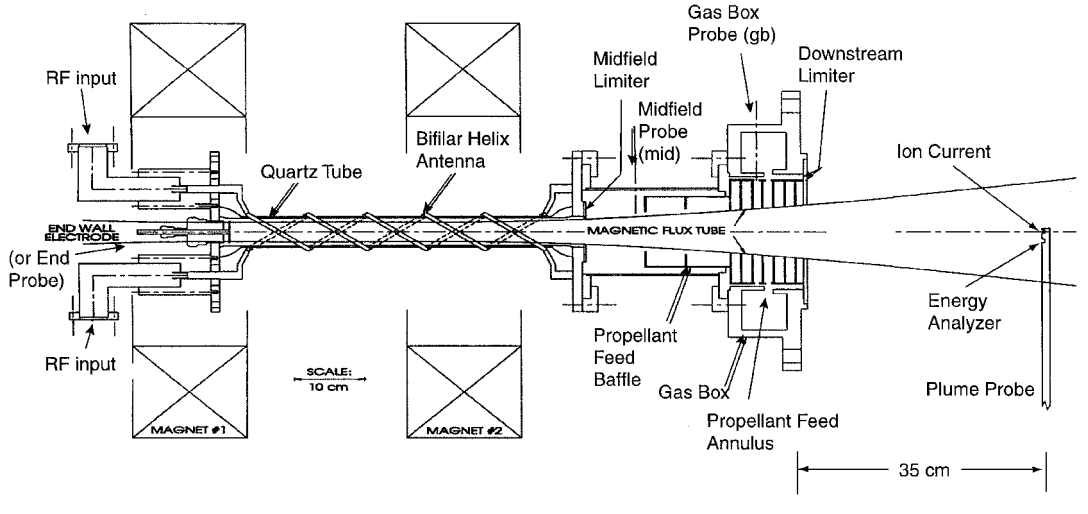

Fig. 1 Experimental thruster and probe diagnostics.

This rf power was coupled through an impedance matching circuit to the thruster, using coaxial transmission line. One-half of the power out of the matching circuit was fed into each winding of the bifilar helix antenna.

Although the magnets were run continuously, for plasma experiments the thruster was operated in a pulsed mode (typical pulse duration $\Delta t \sim 50$ ms) to avoid the need to provide cooling for continuous operation. The pulse-to-pulse reproducibility was good, and in 50 ms the plasma reached near steady-state conditions. Hydrogen gas propellant was used for most experiments. Limited tests were also done in helium and argon gas. To operate the thruster, propellant gas was continuously injected into the gas box using pulsed piezo-electric gas valves. Simultaneously with slow turn on of the magnetron rf power (~10-ms rise time), the gas valves were pulsed on using a high flow rate, 5-ms prepulse, followed by constant lower rate gas injection. Gas breakdown and plasma formation occurred within 10 ms of turn on of the rf power. The propellant flow rate calibration was determined from the pressure rise within the thruster volume for a given gas pulse duration, pulsed valve voltage, and plenum pressure.

B. Plasma Diagnostics

Various diagnostics were employed to measure thruster performance. To measure the rf fields of the whistler wave, small-diameter, single-turn magnetic loop probes and diode detectors were used. The probes were inserted along a radius at two locations shown in Fig. 1, designated mid and gb probes. These could be oriented for coupling to either axial or azimuthal components of the wave. The probes were moved in radius, for a sequence of test pulses, to obtain radial profiles of the rf wave. The measured rf field profiles were peaked on-axis for these experiments. To measure absorption of the wave at the electron-cyclotron resonance, we used an rf loop inserted in to the plasma axis in the gas box. We then varied the magnetic field over a small range, but sufficient to move the resonance surface through the rf probe location, starting from a higher field where the resonance was downstream from the probe. Figure 2 shows the reduction of the measured rf amplitude, down to the noise level for the measurement, as the resonance moved through the probe.

Thruster plasma density and floating potentials were measured with several single-tip cylindrical langmuir probes located at the midfield and gas box locations.[12,13] A few measurements were also made at the rf input end of the thruster by a probe inserted in place of the end wall disk electrode (end probe). The plasma density was inferred from the ion saturation current to a probe ($n_I \propto J_{\text{I-sat}}/\{T_e/m_i\}^{0.5}$) biased sufficiently negative to collect only ions, and the electron temperature T_e was determined from the electron current characteristic obtained by sweeping the probe bias voltage. The plasma floating potentials were measured from the probe voltage at zero collected current.

During operation of the thruster, noise fluctuations in the floating potential $\delta\tilde{\phi}$ and plasma density $\delta\tilde{n}$ were observed. The nature of these fluctuations was a function of the propellant gas flow and depended on the electrical state of the edge limiters, that is, whether the limiters were held at ground potential or allowed to float to zero collected current. For both limiter configurations, the fluctuation amplitudes decreased at larger propellant flow rate. Their characteristics were the following. For grounded limiter operation, typical fluctuation frequencies of the potential and density signals were 1–2 kHz with high harmonic content. Fluctuation amplitudes varied typically $\delta\tilde{\phi}/\Phi < \pm 0.1$ and $\delta\tilde{n}/n < \pm 0.1$, respectively, at the lowest propellant flow rate. For floated limiter operation, bimodal relaxation behavior between two states was observed, a higher density and lower potential condition vs a lower density and higher potential state. The relaxation frequency and fluctuation amplitudes varied with magnetron power level, the magnetic field magnitude, and the propellant flow rate. The dependence of the bimodal frequency on magnetic field is discussed in Sec. III.B. At low propellant flow rates $\delta\tilde{\phi}/\Phi < \pm 0.05$ and $\delta\tilde{n}/n < \pm 0.1$.

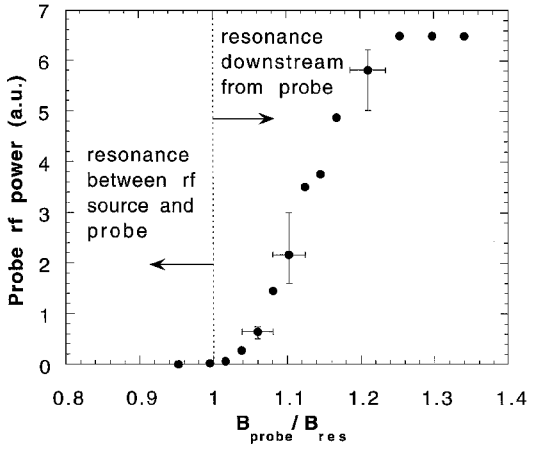

Fig. 2 Measured absorption of rf wave at electron cyclotron resonance.

For the low magnetic fields in our experiments, the probe characteristics were evaluated using probe theory for unmagnetized ions. This assumption is reasonable because the probe radius R_p to ion gyroradius ρ_i ratio was large ($R_p/\rho_i \gg 1$). Fluctuating space potentials can affect the interpretation of probe measurements in plasmas, and the probe data in this experiment were unfiltered for the fluctuation frequency. This permitted measurements of plasma potential and density in both bimodal states.

Fluctuations can lead to several effects: 1) an underestimation of the plasma density determined from ion saturation current measurements and 2) the measured space potential to be more negative than the true value.[14] In our experiment, because $\delta\tilde{\phi} < T_e$, determination of the electron temperature from the slope of $\mathrm{d}/\mathrm{d}V_p\{\ell n(J_{\text{ep}})\}$ should be little affected for J_{ep} measured within the exponential region.[13] To determine the ion saturation current at large negative bias, Lam theory[12] was used. This was cross checked against the more accurate theory of Chen.[13] From these comparisons, the estimated accuracy of densities and temperatures were about 20 and 10%, respectively. The close agreement between the measured maximum plume ion energy and the plasma potential, estimated from the sum of the floating potential and the sheath potential Φ_s, supports this contention (see Sec. II.D).

To measure plasma ions within the plasma exhaust plume escaping out one end in the expanding magnetic field, we used a small current collector probe ($\frac{3}{16}$ in. diam), which could be moved across the plume (plume probe), passing through the thruster axis. The plume probe was located $\Delta z_{\text{pl}} = 35$ cm downstream from the downstream limiter, as shown in Fig. 1. This probe was constructed with two collectors. One was biased to large negative potential to collect the total ion current. The second collector employed two grids in front of the collector, one to provide a ground plane and the other biased with variable positive potential to measure the energy spectrum of escaping ions.[9]

C. Grounded vs Floating Edge Potential

For the whistler wave thruster, we observed a strong dependency of the operating density on the plasma edge potential. When the edge limiters were allowed to electrically float, by connecting them to ground through a high impedance, the ion saturation current measured within the gas box increased a factor ~2.5–3 compared to grounded limiter operation. The variation of the ion saturation current density with the propellant flow rate is plotted in Fig. 3. Equilibrium values for each data point were measured at fixed device parameters (rf power, magnetic field, and propellant flow rate). A data scan consisted of measurements for a sequence of test shots as device parameters, for example, propellant flow rate, were varied. From the probe current collecting area and the electron temperature, the inferred density reached $n_i \sim 1.6 \times 10^{12}$ cm^{-3} at low propellant feed for floated limiters. At this density, the plasma was highly overdense and reached $n_e \sim 100 n_{\text{ec}}$. Note that tests with insulating limiters in helicon source experiments also increased the operating density compared to grounded limiters.[15] These results were unexplained.

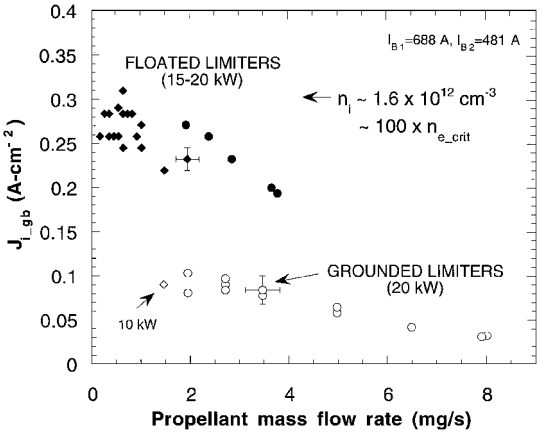

Fig. 3 Dependence of propellant mass flow rate of gas box ion current density for grounded and floating edge limiters.

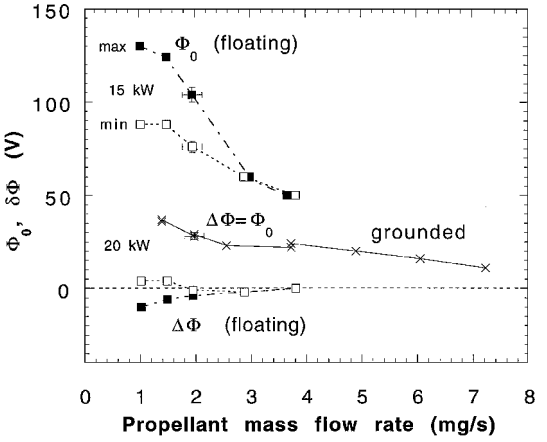

Fig. 4 Probe floating potentials on-axis, Φ_0, and axis-edge difference, $\Delta\Phi$, for grounded and floating edge limiters.

The plasma floating potentials in the gas box increased when the limiters were floated. The potentials were measured on-axis in the gas box and in the edge, by the propellant feed baffle potential. Figure 4 shows the dependence on propellant feed of the measured floating potential Φ_0 for the probe located on the magnetic axis (gas box probe). Within the thruster, this was the axial position with the highest measured floating potential (see Fig. 1 of Ref. 9). Also plotted is the potential difference $\Delta\Phi = \Phi_0 - \Phi_b$, between the on-axis probe, Φ_0, and the propellant feed baffle, Φ_b, at the same axial location. For grounded limiters ($\Phi_b = 0$), $\Phi_0 \leq 40$ V. When the limiters were floated, Φ_0 increased to ~90–130 V at the lowest propellant flow rate. However, the potential difference was much lower, $|\Delta\Phi| < 5$ V, for floating limiters, compared to $\Delta\Phi$ ($=\Phi_0$) ≤ 40 V for grounded limiters.

Smaller $\Delta\Phi$ with floating limiters implies that, for grounded limiters, the radial ion losses exceeded the electron radial losses. The ion acceleration along the magnetic field lines results from the ambipolar electric fields in the plasma, which are generated by escaping heated electrons. This yields an electrostatic potential between the microwave heating zone and the downstream plasma plume, which reaches laboratory ground potential. If conducting limiters at the plasma edge are grounded, it forces the local potentials to ground potential. The result is to induce a radial potential drop in the plasma and to force the potential drop (and ion acceleration) along the field lines to vary with radial position in the plasma. Ambipolar balance must include radial ion losses, which we will show are generated by orbits of newly ionized (and charge exchanged) ions in the radial electric field. Floating the limiters relaxes this constraint, reducing the radial electric field and allowing the thruster to operate in a mode with lower radial ion losses so that ion losses along field lines dominate at all radii. From these results, we conclude that the potential difference $\Delta\Phi$ ($E_r \sim \Delta\Phi$) controls the radial transport of the ions.

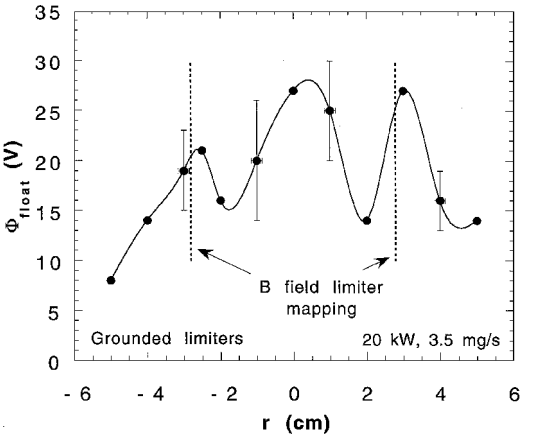

Fig. 5 Time-averaged, floating potential radial profile at the midfield position for grounded limiters.

The actual plasma potential exceeds the floating potential. If the electron energy distribution function were Maxwellian, the expected plasma potential exceeds the floating potential by the probe sheath potential $\Phi_S \sim 0.5 T_e \ln(m_i/m_e)$ (Ref. 16). For the measured electron temperature range ($T_e \sim 10$–20 eV), this added potential is $\Phi_S \sim 40$–80 V. The data for floating limiters labeled min and max in Fig. 4 refer to different potentials observed for bimodal operation. From the results in Fig. 4 it is clear that the radial electric fields are much smaller for floating limiters than for grounded limiters.

For our experiment, we have measured the radial profile of the floating potential with grounded limiters for moderate propellant feed. Figure 5 shows the profile at 3.5 mg/s propellant flow rate measured by the midfield probe scanned across the plasma column between the midfield limiter and the gas box. At this location, a 4.7-cm radial gap and an 8-cm distance along the magnetic field separates the plasma edge from the nearest grounded boundary, so that the local edge potential is not forced to zero. The plasma potentials were noisy, but the time-averaged values (~few millisecond average) plotted in Fig. 5 show radial structure in the profile and a larger potential on the axis than at the plasma edge. We have no measurements of the radial profile of T_e for these data, and so we cannot estimate the variation of Φ with radius to determine the true plasma potential. By the use of the floating potential, the radial electric field within the plasma is in the range $E_r \sim 5$–10 V/cm, and this is probably a lower limit. At lower propellant flow rate, the potentials (and probably E_r) are higher. The increase in ionized propellant density in the gas box for floating limiters is consistent with improved radial confinement of ions. A comparison of the ion saturation current density in the gas box with that at the midfield probe supports this conclusion.

The plasma density measured in the higher magnetic field regions near the antenna by the end probe and by the midfield probe were greater than the gas box density. At the measured density, it is plausible that substantial ionization of neutrals by electron impact extended beyond the propellant feed baffle into the antenna region. The mean free path for ionization of neutrals can satisfy $\lambda_0 \gg a$ (~2–3 cm) depending on the neutral energy. Here, λ_0 ranges from ~5–10 cm for room temperature molecular neutrals to 50–100 cm for more energetic atomic neutrals produced by dissociation. Following ionization, the ions then flowed out the ends or radially. Beyond the stagnation point for ion flow (upstream vs downstream flow), in the absence of radial transport losses between the midfield and gas box locations, particle conservation requires the ratio $J_{i\text{-}gb}/J_{i\text{-}mid} \geq B_{gb}/B_{mid}$, where J_i and B are local values of the ion current density and the magnetic field, respectively. Figure 6 compares this ratio for grounded and floating limiter operation. For grounded limiters (Fig. 6a) $J_{i\text{-}gb}/J_{i\text{-}mid} < B_{gb}/B_{mid}$, consistent with large radial ion losses. When the limiters were floating, the ratio is much greater and $J_{i\text{-}gb}/J_{i\text{-}mid} \geq B_{gb}/B_{mid}$ (Fig. 6b), consistent with lower radial losses. At the lower propellant flow rates, $J_{i\text{-}gb}/J_{i\text{-}mid} > B_{gb}/B_{mid}$, indicating both low radial losses and ion production from gas ionization between the two points.

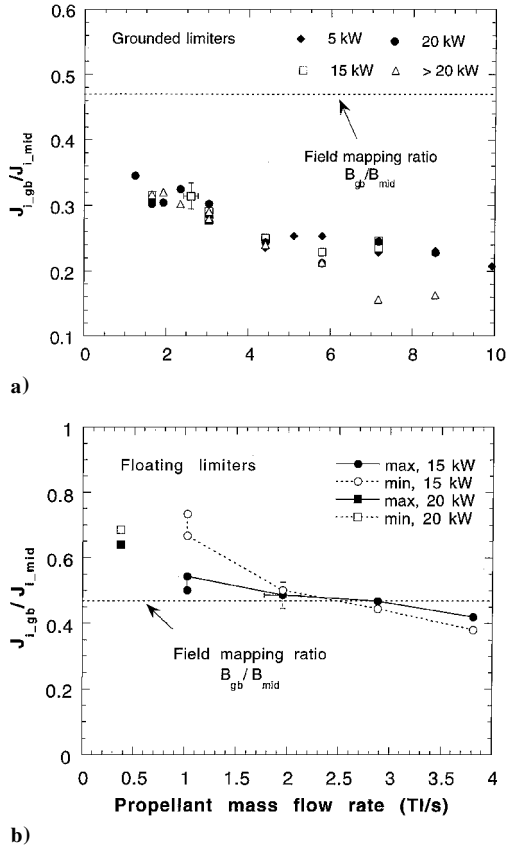

Fig. 6 On-axis ion current density ratio between the gas box and the midfield positions for a) grounded and b) floating limiters.

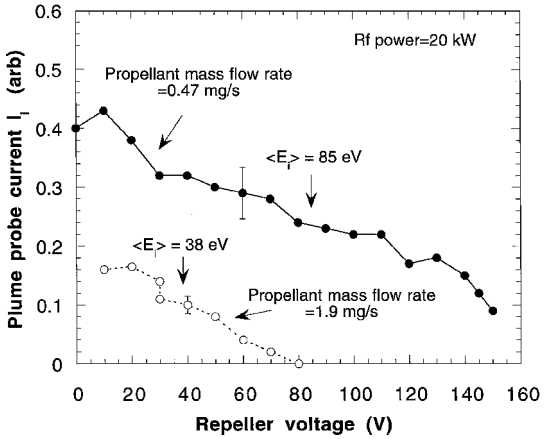

Fig. 7 Plume probe ion current density dependence on repeller voltage with floating limiters for 0.47- and 1.9-mg/s H_2 propellant mass flow rates.

D. Plasma Plume Measurements

The movable plume probe was used to measure the energy spectra of escaping ions, the ion end loss currents, and the transverse dimensions of the plume plasma. We measured ion energy spectra on the magnetic axis for several gas flow rates for floating limiter operation. Figure 7 shows the probe ion current collected when the grid repeller voltage V_r was biased positive. The collected probe current I_p varies as

$$I_p(V_r) \sim \int_{V_r}^{E_{\max}} \sqrt{\frac{E_i}{m_i}} F(E_i)\, \mathrm{d}E_i \qquad (1)$$

At zero bias the probe measured the total ion current density, and the cutoff bias at zero current determined the maximum ion energy. At low propellant flow rates (0.47 mg/s), the maximum plume ion energies reached ~150 eV, corresponding to a peak velocity of 1.2×10^5 m/s for H_2^+. At higher propellant flow rates (1.9 mg/s) both the maximum energy and the collected current decreased. The plume ion energy spectra can be determined from the derivative with respect to V_r of the collected current. For these two spectra, the mean on-axis ion energy $\langle E_i \rangle$ for the plume ions was 85 eV for low propellant flow rate and 38 eV for the higher propellant flow rate. If the plume ion energy spectra were uniform in radius and the ions were H_2^+, the corresponding values of specific impulse would be 9200 and 6100 s, respectively.

From the shape of the spectra in Fig. 7, it is apparent that the ion energy distribution is broad. Broadening of the energy distribution can arise from several processes. A spread in perpendicular ion energy because of ion orbit drifts within the radial ion potential well, as discussed in Sec. III, will produce a spread in axial energy from ∇B forces as the ions move down the potential into the plume. There may also be charge exchange on un-ionized propellant gas from the gas box in the expanding plume. As ions exit the gas box and accelerate down the potential hill, charge exchange creates a cold ion part way down the potential fall between the gas box and the plume probe. Although the total ion current does not change with charge exchange, the new ion will reach the probe with a lower energy than ions that do not charge exchange. With large uncertainty, the estimated probability of charge exchange in the distance Δz_{pl} to the plume probe is $\Delta z_{\mathrm{pl}}/\lambda_{\mathrm{cx}} \sim 0.5$ at the low propellant flow rate. This probability is large enough to produce a large ion energy spread at the plume probe.

Even with electrically floating limiters inside the thruster, the ion radial confinement was poor in the plasma plume output of the thruster. This was evident from the plasma plume measurements. Comparing the on-axis ratio of ion current flow at the plume probe to that in the gas box, it falls well below the ratio obtained from magnetic flux tube divergence (Fig. 8), a result consistent with a large radial loss. Even though the gas box and limiters were floating for this measurement, downstream from the gas box in the region of the expanding plasma plume there were no electrically floating electrodes at the plasma boundary. The boundary walls were grounded, but well separated from the plasma edge (>10 cm). Unfortunately, no potential profile measurements were made within the plume to estimate the radial electric fields. Note that the measured transmitted ion current ratio, $J_{\mathrm{i\text{-}pl}}/J_{\mathrm{i\text{-}gb}}$, was a maximum when the floating potential of the gas box was minimum (filled data points labeled $\Phi_{\min}$ in Fig. 8) for the bimodal behavior. Because the ratio varied with the potential, the dependence of ion plume current on the potential was not just a change with potential of the ion current density exiting the gas box. The inverse relation between higher potential (and probably higher radial electric field) and lower plume current, suggests again that the radial electric field strongly influenced ion radial confinement within the exhaust plume.

For floating limiters, the plume ion current profile (Fig. 9) shows a central core and a surrounding halo containing an estimated ~50% of the total current. The central core of the plasma plume matches

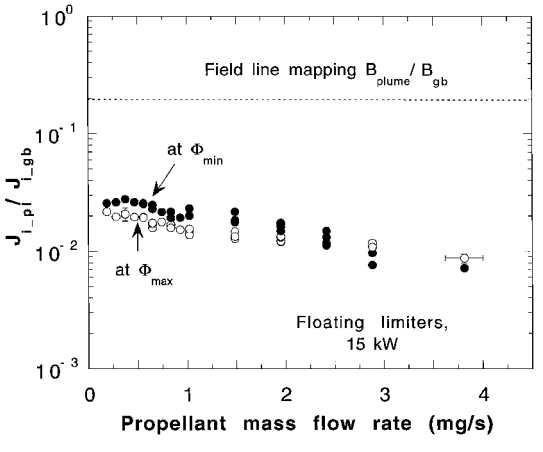

Fig. 8 Ratio of plasma plume probe to gas box probe ion current density.

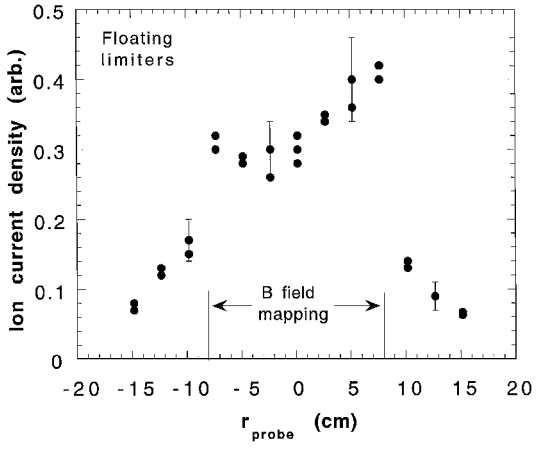

Fig. 9 Radial profile of plume ion current density for floating limiters (15 kW and 2.0 mg/s propellant mass flow rate).

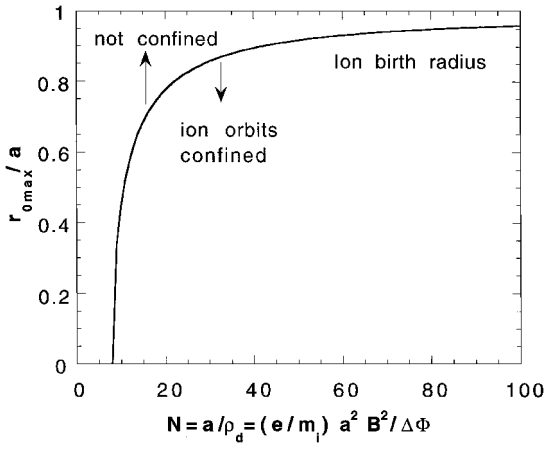

Fig. 10 Normalized ion birth radius for confined orbits in a parabolic potential profile.

the diameter inferred from the magnetic field line mapping of the magnetic flux tube exiting the gas box limiter. The halo current is consistent with large ion orbits and a radial transport process.

III. Role of E_r for Transport

A. Ion Orbits and Model Predictions

The picture that emerges from the data is that the radial electric E_r has a very strong effect on both the plasma potential and the ion confinement and, therefore, the plasma density. It is instructive for understanding the radial transport to examine the effects of E_r on ion orbits. To estimate the magnitude of effects, we first consider a simple slab model with a uniform perpendicular electric field E_r within a uniform axial magnetic field B_z. In these fields both ions and electrons perform cyclical orbits in the x–y plane and drift ($E \times B$ vector cross product) in the y (azimuthal coordinate) direction with an average gyrocenter velocity given by E_r/B_z. For singly charged ions born at rest, the ion drift orbit radius and the perpendiculardrift energy, averaged over the orbit, are given by $\rho_d = (m_i/e)E_r/B_z^2$ and $\langle W_{i\perp}\rangle = \rho_d(eE_r)$, respectively. For our thruster experiments, the electron-cyclotron resonance field $B_{\rm res} = 0.0327$ T in the gas box (rf frequency = 915 MHz), and using estimated radial electric fields $E_r \sim 10$–20 V/cm, the ion orbit size and average drift energy vary from $\rho_d = 2$ to 4 cm and from $\langle W_{i\perp}\rangle \sim 20$ to 80 eV, respectively, for H_2^+ ions. This orbit size is a substantial fraction of the plasma radius in the gas box ($a \sim 4.0$ cm), and the average ion drift energy is large.

The consequences of large orbits ($\rho_d \sim a$) and large perpendicular drift energies are poor particle and energy confinement. For typical thruster operating parameters, charge exchange dominates interactions with neutrals. There are two effects.

1) Cold ions born by electron impact ionization of neutrals, or by charge exchange of existing ions with neutrals, can be lost radially if their ionization point occurs at a radius where the orbits are not confined radially.

2) Charge exchange causes loss of energetic neutrals with tens of electron volts perpendicular drift energy, leaving behind a cold, and possibly unconfined, ion.

For fixed operating potential, these losses decrease at higher magnetic field and larger plasma radius, as shown by the simple relations for slab geometry. For a nonuniform electric field, the ion orbits are a sensitive function of the electric field profile in the plasma. To estimate the effect of nonuniform fields, we solve the ion equations of motion in cylindrical coordinates (r, θ), neglecting changes along the magnetic axis. The equations for total energy and angular momentum are

$$\frac{1}{2}m_i\left(\frac{dr}{dt}\right)^2 + \frac{1}{2}m_i\left(r\frac{d\theta}{dt}\right)^2 + [e\Phi(r) - e\Phi(r_0)] = 0 \quad (2a)$$

$$\frac{d}{dt}\left(m_i r^2\frac{d\theta}{dt}\right) = -eB_z r\frac{dr}{dt} = -\frac{1}{2}\frac{d}{dt}\left(eB_z r^2\right) \quad (2b)$$

where the initial conditions at $t = 0$ are $r = r_0$, $dr/dt = 0$, and $d\theta/dt = 0$. Ion orbits can be characterized by an ion orbit size parameter, $N = a/\rho_d$, where N is the number of ion orbit drift radii within the plasma radius a and $\rho_d = (m_i/e)(\Delta\Phi/a)(1/B_z^2)$. N is given by

$$N = (e/m_i)a^2B_z^2\big/\Delta\Phi \quad (3)$$

where $\Delta\Phi/a$ is the average electric field.

Rewriting Eq. (2a) with the parameter N and using the constancy of canonical angular momentum implied from Eq. (2b), we have the following equations:

$$\left(\frac{dr}{dt}\right)^2 = \left(\frac{2\omega_{ci}^2 r_0^2}{N}\right)\left\{\left(\frac{a}{r_0}\right)^2\left[\frac{d\phi}{\Delta\Phi}\right] - \left(\frac{N}{8}\right)\left[\left(\frac{r}{r_0}\right) - \left(\frac{r_0}{r}\right)\right]^2\right\} \quad (4a)$$

$$\frac{d\theta}{dt} = -\left(\frac{\omega_{ci}}{2}\right)\left[1 - \left(\frac{r_0}{r}\right)^2\right] \quad (4b)$$

where $\omega_{ci} = eB_z/m_i$ is the ion Larmor frequency and $d\phi = \Phi(r_0) - \Phi(r)$. Solution of Eq. (4a) for $dr/dt = 0$ determines the outer turning point for the ion orbit, $r = r_{tp}$, where dr/dt changes sign from positive to negative.

Consider a specific example for an assumed parabolic radial potential profile $\Phi = \Delta\Phi[1 - (r/a)^2]$. Figure 10 shows the maximum normalized birth radius $r_{0\max}/a$ for confined ion orbits, satisfying $r_{tp} \le a$, plotted against N. The curve, given by $r_{0\max}/a = [1 - 8/N]^{0.5}$, is the maximum birth radius for confined ions. Ions with birth radii $r_0 < r_{0\max}$ are confined. For this example, ions are no longer confined for $N < 8$, but the maximum radius for confined ion orbit increases rapidly with N. From Eq. (4), the orbit trajectory can be found from the solution of the integral equation

$$\theta(r) = \int_{r_0}^{r}\left(\frac{d\theta}{dr}\right)dr \quad (5)$$

The trajectories in Fig. 11a show the ion orbits for several ion birth radii for $N = 12$. The last confined orbit has a birth radius $r_0/a = 0.5773$. The rapid increase in orbit size for smaller N is shown in Fig. 11b for birth radius $r_0/a = 0.2$. The curves in Fig. 11b show one-half of the orbit trajectory, between the inner and outer turning points. As N approaches 8, an ion circulates a greater angle about the axis for a complete orbit.

B. Experimental Scaling

The ion orbit calculations demonstrate the significance of radial electric fields for thruster performance. For the experiments described the estimated values of the orbit parameter N at the lowest propellant flow rates vary from $N \sim 2$–3 for grounded limiters

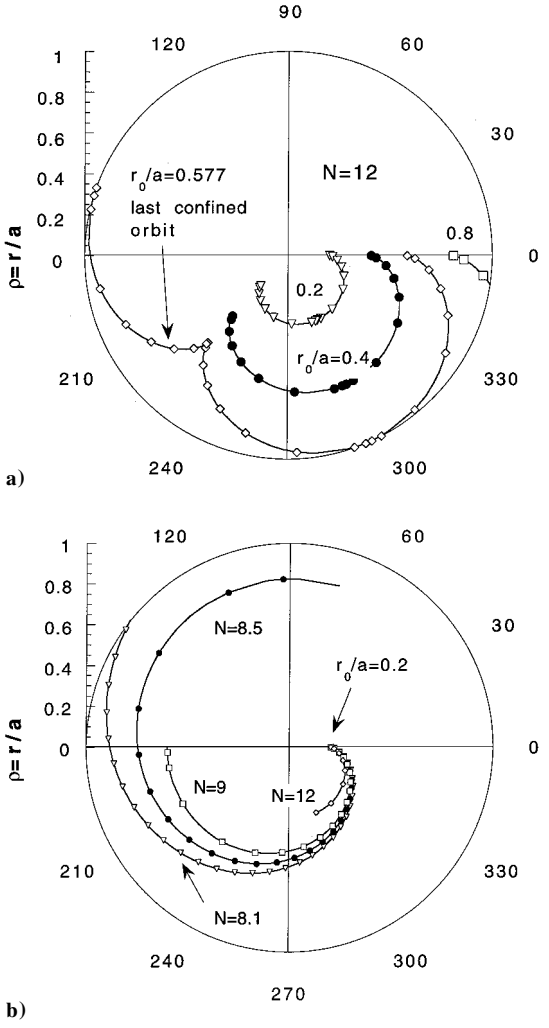

Fig. 11 Ion orbit for parabolic potential: a) $N = 12$ and b) ion birth radius $r_0/a = 0.2$.

to $N \sim 10$–20 when the limiters were floating. The curve shown in Fig. 10 for a model parabolic potential profile predicts a large increase in the volume of confined ion orbits for floating limiters, consistent with experimental observations. The parabolic model prediction and the orbit trajectories shown in Fig. 11 provide only crude estimates of the ion orbits because we have only limited knowledge of the actual potential profiles. In addition, the assumption of uniformity along the magnetic axis is violated. During one orbit period, the ions in the exhaust plume experience axial acceleration down the magnetic field from both ∇B and $\nabla\Phi$ forces. As they move into the region of weaker field, the ion orbit size increases. However, because the ion axial velocity increases, the ions can provide thrust if they do not strike a surface before escaping from the flight vehicle.

An obvious method to improve thruster performance is to increase the parameter N. This can be done by raising the magnetic field (and operating frequency f) or increasing the radial dimensions of the plasma column. During our experiments we operated the thruster over a range of magnetic field with the frequency and the magnetic field shape held constant. For these experiments, the edge limiters and gas box were floating. Thruster performance was not optimized because the axial location of electron-cyclotron resonance moved within the propellant feed box. Nevertheless, the ion saturation current density strongly increased with B. Figure 12a shows the increase at the midfield and gas box locations. The increase was greatest at the weaker field position in the gas box ($B \sim 0.03$ T), $J \sim B^{1.7}$, consistent with ion orbit theory and smaller N. At the higher field location ($B \sim 0.09$ T), the current density increase with B was weaker, as expected from the orbit calculations.

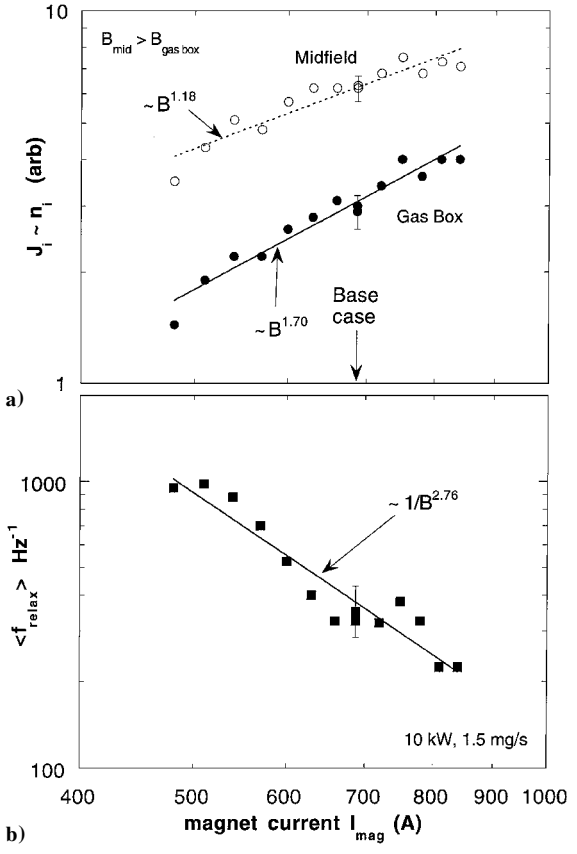

Fig. 12 Magnetic field scaling of a) ion current density and b) bimodal relaxation frequency.

As discussed in Sec. II.B, the thruster operation at lower propellant flow rates was bimodal, switching between two states with an average relaxation rate frequency $\langle f_{\text{relax}} \rangle$. This characteristic was particularly visible in the probe measurements of ion saturation current density and floating potentials. The current switched between a high and a low current state, and the potentials also oscillated, but out of phase with the current from a lower to a higher value. When we varied the magnetic field, f_{relax} decreased very strongly with B ($\langle f_{\text{relax}} \rangle \sim 1/B^{2.8}$), as plotted in Fig. 12b. Whereas this behavior is not well understood, it is probable that the relation between E_r and ion radial confinement played a dominant role in the plasma stability.

These conclusions suggest that poor ion radial confinement may have degraded efficiency in previous ECH thruster experiments with heavy ions because of small values of the parameter N (estimate $N \sim 1$ for small a and large E_r and A_I) (Ref. 5).

IV. Conclusions

The reanalysis of experimental results for the whistler wave plasma thruster presented here suggests several ways to improve significantly the thruster efficiency. Modest increases in the operating frequency (and magnetic field) and/or the plasma column diameter will increase the orbit parameter N, the ion radial confinement, and the plasma density. Higher density and reduced neutral gas mean free path λ_0 should increase the percentage ionization of the injected propellant. At the same time, with larger N the ion drift energy $\langle W_{i\perp} \rangle$ will decrease, and the power loss of energetic neutrals by charge exchange of these ions on neutral gas will be much less important. An extension into the plume of edge electrodes to reduce the radial potential difference $\Delta\Phi$ and E_r should both increase the axial throughput of ions and improve the axial directivity of ion momentum in the exhaust plume.

By the use of these methods, the projected increase in ion flow efficiency into the plume may be crudely estimated. Several steps to increase efficiency should be investigated. First, for the present operation with floated limiters at the lowest propellant flow rates

(~0.5 mg/s), the measured ion saturation current on-axis in Fig. 3 reached $J_{i0} \sim 0.3$ A/cm^2. The total ion current flow out of the gas box was $I_{\text{itot}} = A_{\text{eff}} J_{i0} \approx 13$ A, using a current-weighted effective gas box cross-sectional area, $A_{\text{eff}} \approx 42$ cm^2, obtained from radial profile measurements of ion saturation current in the gas box. Without knowledge of the ion species mix, a precise propellant efficiency or exhaust thrust cannot be determined. If H_2^+ ions were dominant, the ion flow rate corresponds to a propellant flow rate ≈0.27 mg/s, an approximate 50% propellant ionization efficiency. If radial transport losses in the plume were also made very small by extending floating edge limiters out into the exhaust plume, ion current in the exhaust plume could approach the gas box output. Ion plume energy spectra measurements are available only on-axis. If off-axis values were similar, consistent with $\Delta\Phi/\Phi_{\text{gb}} \ll 1$ for floating edge limiters, the plume exhaust ion power flow becomes $P_{\text{iex}} \approx I_{\text{itot}}\, \Phi_{\text{gb}} \approx 2.0$ kW, for typical 12-kW rf power coupled into the antenna. To produce each ion–electron pair in hydrogen, a minimum energy $\Delta W_{\text{ie}} \sim 30$–$40$ eV is required,[17] implying an overall minimum ion power efficiency $\sim \frac{2.4}{12} = 0.24$. Second, by the increase of operating magnetic field and frequency and/or the increase of the plasma radius, the data in Fig. 12 indicate further increases in the density, ion current flow from the gas box, and power flow into the plume are expected. With full propellant ionization efficiency, ion power efficiency approaches 50%.

The bifilar helix antenna used in the experiments reported here was not optimized, and this region of the plasma was poorly diagnosed. The power coupling efficiency from the rf magnetron into the antenna was large (typically ≥80–90%), but the power fraction coupled to the whistler wave is uncertain and not optimized. Further experiments to optimize antenna geometry, higher frequency, and larger plasma diameter are required to investigate these issues. Energy losses due to recycling at the high field end of the thruster are minimized by the magnetic geometry (high magnetic field) and the anisotropic electron distribution. These losses are estimated to reduce the power efficiency by about 10% (Ref. 8).

Acknowledgments

This work was performed under the auspices of the U.S. Department of Energy by Lawrence Livermore National Laboratory under Contract W-7405-ENG-48 and of the NASA John H. Glenn Research Center at Lewis Field.

References

[1]Martinez-Sanchez, M., and Pollard, J. E., "Spacecraft Electric Propulsion-An Overview," *Journal of Propulsion and Power*, Vol. 14, No. 5, 1998, pp. 688–699.

[2]Brophy, J. R., and Noca, M., " Electric Propulsion for Solar System Exploration," *Journal of Propulsion and Power*, Vol. 14, No. 5, 1998, pp. 700–707.

[3]Stix, T. J., *The Theory of Plasma Waves*, American Inst. of Physics, Woodbury, New York, 1992, p. 40.

[4]Harvey, B. M., and Lashmore-Davies, C. N., "The Absorption Mechanisms of Whistler Waves in Cool, Dense, Cylindrically Bounded Plasmas," *Physics of Fluids*, B, Vol. 5, No. 12, 1993, pp. 3864–3875.

[5]Kosmahl, H. G., Miller, D. B., and Bethke, G. W., "Plasma Acceleration with Microwaves Near Cyclotron Resonance," *Journal of Applied Physics*, Vol. 38, No. 12, 1967, pp. 4576–4582.

[6]Sercel, J. C., "Electron-Cyclotron-Resonance (ECR) Plasma Acceleration," AIAA Paper 87-1407, June 1987.

[7]Sercel, J. C., "Electron-Cyclotron-Resonance (ECR) Plasma Thruster Research," AIAA Paper 88-2916, July 1988.

[8]Hooper, E. B., Jr., "Plasma Flow Resulting from Electron Cyclotron Resonance Heating on a Magnetic Hill," *Physics of Plasmas*, Vol. 2, No. 12, 1995, pp. 4563–4569.

[9]Stallard, B. W., Hooper, E. B., and Power, J. L., "Whistler-Driven, Electron-Cyclotron-Resonance-Heated Thruster: Experimental Status," *Journal of Propulsion and Power*, Vol. 12, No. 4, 1996, pp. 814–816.

[10]Stallard, B. W., and Hooper, E. B., Jr., "A Re-Appraisal of the Whistler Wave Thruster," *Ninth Advanced Space Propulsion Workshop*, Jet Propulsion Laboratory, JPL Rept. D-15671, March 1998.

[11]Burrell, K., "Effects of $E \times B$ Velocity Shear and Magnetic Shear on Turbulence and Transport in Magnetic Confinement Devices," *Physics of Plasmas*, Vol. 4, No. 5, 1997, pp. 1499–1518.

[12]Lam, S. H., "Unified Theory for the Langmuir Probe in a Collisionless Plasma," *Physics of Fluids*, Vol. 8, No. 1, 1965, pp. 73–87.

[13]Chen, F. F., "Numerical Computations for Ion Probe Characteristics in a Collisionless Plasma," *Plasma Physics*, Vol. 7, 1965, pp. 47–67.

[14]Garscadden, A., and Emeleus, K. G., "Notes on the Effect of Noise on Langmuir Probe Characteristics," *Proceedings of the Physical Society*, London, Vol. 79, 1962, pp. 535–541.

[15]Chevalier, G., and Chen, F. F., " Experimental Modeling of Inductive Discharges," *Journal of Vacuum, Science Technology* A, Vol. 4, No. 11, 1993, pp. 1165–1171.

[16]Hutchinson, I. H., *Principles of Plasma Diagnostics*, Cambridge Univ. Press, New York, 1987, Chap. 3.2.

[17]von Engel, A., *Ionized gases*, 2nd ed., Oxford at the Clarendon Press, London, 1965, pp. 179–183.